ASIDE

ASIDE Cardiovascular

ASIDE CARDIOVASCULAR

Original Article

Ac-SDKP Maintains Coronary Microvascular Barrier Function and Prevents Radiation-induced Cardiac Injury

Sarmila Nepali[1], Badri Karthikeyan[1], Swati D Sonkawade[2], Supriya D Mahajan[2], Joseph Spernyak[3], Umesh C Sharma[3], Saraswati Pokharel[1,*]

1-Department of Pathology and Laboratory Medicine, Roswell Park Comprehensive Cancer Center, Buffalo, NY, USA
2-Department of Medicine, Jacob's School of Medicine and Biomedical Sciences, University at Buffalo, Buffalo, NY, USA
3-Translational Imaging Shared Resources, Roswell Park Comprehensive Cancer Center, Buffalo, NY, USA

ARTICLE INFO

Article history:
Received 26 Mar. 2026
Received in revised form 17 Apr. 2026
Accepted 21 Apr. 2026
Published 13 May 2026

Keywords:
Radiation
Cardiomyopathy
Ac-SDKP
Claudin-1
Endothelial dysfunction
Vascular permeability

ABSTRACT

Background: Radiation-induced cardiomyopathy is a significant late complication in cancer survivors treated with thoracic radiation, with few preventive options. Early injury is characterized by coronary microvascular endothelial dysfunction and increased vascular permeability. Claudin 1 (Cldn1), a tight junction protein in endothelial cells, plays a key role in maintaining vascular barrier integrity. This study investigated whether the endogenous tetrapeptide N acetyl Ser Asp Lys Pro (Ac SDKP) preserves cardiac microvascular barrier function and mitigates early radiation-associated cardiac injury in preclinical models.

Methods: Human coronary microvascular endothelial cells (HMVECs) were exposed to ionizing radiation (IR) with preventive Ac SDKP treatment. Endothelial barrier function was assessed using FITC dextran permeability and transendothelial electrical resistance (TEER). In vivo, mice received fractionated left thoracic irradiation (3 Gy/day, 5 days/week; total 45 Gy). Ac SDKP (3.2 mg/kg/day) was administered via a subcutaneous osmotic minipump, starting 1 day prior to irradiation and continuing throughout the study. Cardiac vascular leakage was measured by Evans blue extravasation at early and chronic time points, and left ventricular (LV) function was evaluated by cardiac MRI.

Results: IR decreased Cldn1 expression, increased endothelial permeability, and reduced TEER in HMVECs. Preventive Ac SDKP preserved Cldn1 expression and significantly reduced IR-induced permeability, although TEER recovery was partial. In mice, irradiation reduced cardiac Cldn1 levels, increased vascular leakage, and impaired LV function. Ac SDKP reduced early leakage and improved selected functional measures, with no significant effect on chronic permeability.

Conclusion: Preventive Ac SDKP attenuates radiation-related cardiac microvascular dysfunction and partially preserves cardiac function, likely through maintenance of endothelial barrier integrity and Cldn1 expression, suggesting potential vascular protective pathways.

1. Introduction

Thoracic radiation therapy (RT) is one of the major treatment modalities for various cancers, including breast, lung, and mediastinal malignancies [1]. However, incidental exposure of the heart to ionizing radiation (IR) is a well-established contributor to radiation-induced heart disease (RIHD), often presenting as delayed cardiovascular toxicity [2]. Clinical and experimental evidence suggests that microvascular injury is among the earliest events in the pathogenesis of RIHD. In particular, disruption of the coronary microvascular endothelial barrier often precedes myocardial inflammation, fibrosis, and contractile dysfunction [3].

The endothelial barrier is tightly regulated by intercellular junctional complexes, of which tight junctions (TJs) are essential components[4]. TJs are formed by transmembrane proteins, including occludins, junctional adhesion molecules, and claudins, which work collectively to restrict paracellular flux and maintain vascular homeostasis [5]. Among these, claudin-1 (Cldn1) is an important TJ protein implicated in barrier integrity by forming selective channels that regulate solute and ion permeability [6, 7]. While Cldn1 has been extensively characterized in epithelial tissues, its role in cardiac vasculature is less well understood. We recently demonstrated that claudin 1 (Cldn1) is enriched in coronary microvascular endothelial cells and that chest irradiation reduces its mRNA and protein expression [8]. However, those studies primarily focused on structural remodeling and myocardial blood flow. They did not address whether Cldn1 is a candidate pathway involved in radiation-induced vascular leakage, or whether restoring Cldn1 is associated with improved radiation-induced disruption of the cardiac vascular barrier. Increased vascular permeability can promote myocardial edema and tissue remodeling, ultimately contributing to ventricular dysfunction [9]. Identifying agents that preserve endothelial barrier integrity may therefore offer new strategies to prevent or mitigate radiation induced cardiac injury.

* Corresponding author: Saraswati Pokharel, Department of Pathology and Laboratory Medicine, Roswell Park Comprehensive Cancer Center, Buffalo, NY, USA. Email: saraswati.pokharel@roswellpark.org

Published and owned by PubPorta Publishing LLC. Academic oversight and scholarly guidance are provided by the American Society for Inclusion, Diversity, and Equity in Healthcare (ASIDE). ISSN (Print) 3069-9851, ISSN (Online) 3069-9843. ©2026 The Author(s). This is an open-access article distributed under the terms of the Creative Commons Attribution 4.0 International License (CC BY 4.0). Hosting by ASIDE Journals.

Citation: Nepali S, Karthikeyan B, D Sonkawade S, et al. Ac-SDKP maintains coronary microvascular barrier function and prevents radiation-induced cardiac injury. ASIDE Cardiovasc. 2026;1(2):9-18, doi:10.71079/ASIDE.CV.051326685

Consistent with this gap, our prior studies examining AcSDKP in radiation-induced cardiac injury focused predominantly on late myocardial remodeling outcomes, including fibrosis and coronary blood flow, without directly assessing early vascular barrier dysfunction or endothelial cell tight-junction integrity. Whether radiation disrupts cardiac vascular endothelial barrier functions early, and whether these early changes contribute to later cardiac injury, remains incompletely defined.

N-acetyl-Ser-Asp-Lys-Pro (Ac-SDKP) is an endogenous tetrapeptide generated through the enzymatic hydrolysis of its precursor, thymosin 4 [10]. Although primarily synthesized in the bone marrow and mononuclear cells, Ac-SDKP has also been detected in various organs, including the heart, kidneys, and vasculature [11–13]. We have previously demonstrated that Ac-SDKP exerts potent anti-inflammatory and antifibrotic effects in preclinical models of cardiac fibrosis [14, 15]. In our most recent work, we identified additional protective actions of Ac-SDKP in reducing myocardial fibrosis and enhancing coronary blood flow following chest irradiation [16]. While Ac-SDKP has been shown to preserve endothelial function in multiple organ systems, its effects on endothelial barrier integrity, especially in the context of radiation-induced vascular injury, remain poorly understood.

In this study, we investigated whether radiation-induced down-regulation of Cldn1 is associated with impairment of the cardiac vascular endothelial barrier and whether Ac-SDKP can attenuate these changes. Using in vitro and in vivo models, we evaluated endothelial permeability, cardiac vascular leak, and cardiac function to determine whether preservation of barrier integrity is associated with Ac SDKP – mediated protection following thoracic irradiation.

Our findings indicate that Ac-SDKP could mitigate radiation-induced cardiac vascular injury while concurrently preserving Cldn1 expression.

2. Methods

2.1. Cell culture and irradiation

Human Cardiac Microvascular Endothelial Cells (HMVECs) (Lonza, CC-7030) were cultured in EGM-2MV medium (Lonza, CC-3156) supplemented with the EGM-2V BulletKit (Lonza, CC-3202) at 37°C in a humidified incubator with 5% CO. For irradiation experiments, HMVECs were seeded at 2×10 cells per well in 12-well insert plates (Corning, 3460) and incubated for 24 hours. The medium was then replaced, and a subgroup of cells was treated with Ac-SDKP (100 nM) for 4 hours prior to irradiation. Cells were subsequently exposed to 9 Gy of ionizing radiation using a specialized orthovoltage radiation chamber, as previously described [17]. Following irradiation, cells were returned to standard culture conditions for an additional 48-72 hours before additional assays.

2.2. In vitro permeability assay

Seventy-two hours after irradiation, HMVECs were subjected to a permeability assay using fluorescein isothiocyanate (FITC)-dextran (25 μg/mL; Sigma-Aldrich, NC0689651). FITC-dextran was added to each insert, and the plate was incubated in the dark at room temperature for 20 minutes. Following incubation, the inserts were removed, and 100 μL of media from each receiver well was transferred to a 96-well black opaque plate (Greiner Bio-One, 655076). Permeability was quantified by measuring fluorescence intensity at 485 nm excitation and 535 nm emission using a plate reader (Synergy H1, BioTek). Permeability assays were performed in at least three independent experiments, with a total of 10 - 19 sample wells analyzed per condition across all experiments. Replicate wells were averaged, and experiment-level means were used for statistical analysis.

2.3. Animal studies

The animal care and experimental protocols were carried out in accordance with the US National Institutes of Health guidelines and were approved by the Institutional Animal Care and Use Committees of the Roswell Park Comprehensive Cancer Center (Institutional Animal Care and Use Committee #1336M). Both male and female mice (6-7 weeks old) were used for in vivo studies. Mice were euthanized using CO2 overexposure followed by cervical dislocation.

2.4. Mouse radiation therapy

Experimental mice were subjected to fractionated left chest irradiation at a dose of 3 Gy/day, five days per week, for a total of 45 Gy over three weeks. The X-ray beam was targeted to the left thorax using an orthovoltage irradiator equipped with a Thoreau's filter, as previously described [17]. A subset of mice was sacrificed at the end of the three-week radiation protocol for permeability assays. In contrast, a second subset was sacrificed 18-20 weeks after the start of radiation for long-term analysis. Additional age-matched radiation-unexposed mice were used as biological controls. Unilateral left thoracic irradiation was selected to approximate clinically relevant cardiac exposure during thoracic radiotherapy while limiting off-target organ injury and enabling long term survival.

2.5. Ac-SDKP therapy

Ac-SDKP therapy: Mice were treated with continuous subcutaneous infusion of Ac-SDKP (3.2 mg/kg/day) for 3 weeks (acute study) or 18-20 weeks (chronic study) using ALZET® Mini-Osmotic Pumps (infusion was started 24 h before radiation exposure). After the completion of the treatment protocol, animals were sacrificed (with CO2 overexposure), and organs were harvested for additional histopathological and molecular analysis.

2.6. Study design

We used three experimental groups of sex- and age-matched mice (6-7 weeks) for both acute and chronic studies: (I) sham-irradiated control mice, (II) mice receiving thoracic irradiation alone, and (III) mice receiving thoracic irradiation with Ac-SDKP treatment. For the acute study, mice from each group were sacrificed at the early (3 weeks) post-irradiation time point (n = 7-9 per group). For the chronic study, separate cohorts were followed long term (18-20 weeks) and sacrificed at the chronic endpoint (n = 7-9 per group). All animal procedures were performed under anesthesia to minimize discomfort and were conducted in accordance with protocols approved by the Institutional Animal Care and Use Committee (IACUC). Euthanasia was performed in compliance with the guidelines of the Panel on Euthanasia of the American Veterinary Medical Association. All image-based analyses of cardiac imaging, histological, and immunohistochemical quantification were performed by investigators blinded to group allocation. No animals or samples were excluded from analysis unless pre-specified technical criteria were not met, and no post hoc exclusions were applied.

2.7. Cardiac magnetic resonance imaging (MRI) for the assessment of myocardial morphology and function

Between 18 and 20 weeks after IR, a subset of mice was anesthetized and maintained under 2 – 2.5% isoflurane throughout the imaging procedure. Body temperature and vital signs were continuously monitored and controlled using an MR-compatible gating and monitoring system (Model 1025, SA Instruments, Stony Brook, NY). Cardiac-gated steady-state free precession scans were obtained

in apical 2- and 4-chamber views using the following parameters: TE/TR = 2.0/4.0 ms, flip angle = 25°, field of view (FOV) = 4.0 × 2.8 cm, matrix size = 128 × 96, slice thickness = 1 mm, six averages, and 16 frames per cardiac cycle. Left ventricular (LV) volumes and function were analyzed using Segment software (version 3.0 R7732; http://segment.heiberg.se). LV endocardial and epicardial borders were delineated from the short-axis cine images acquired at the mid-papillary muscle level. LV diameters and volumes were estimated geometrically from these images, and volume-versus-time curves were generated across 16 frames to characterize systolic and diastolic phases.

To evaluate time-dependent changes in myocardial contractility, radial velocities were measured across six myocardial segments (anterior, anteroseptal, inferoseptal, inferior, inferolateral, and anterolateral), using the mid-septum as the reference for rotation. The velocity mapping algorithm was validated by comparison with prior Doppler echocardiography data assessing average systolic radial velocities in adult male rodents. Quantitative analysis of radial velocity (cm/s) was performed at peak systole (vS), the maximal point on individual segmental velocity curves, which reflects peak contractile force generation. Acceleration was calculated by taking the time derivative of the radial velocity. This imaging and analysis protocol has been previously validated and published [18].

2.8. In vivo cardiac vascular leakage (Miles' assay)

Miles' assay is based on the intravenous injection of Evans Blue, a dye with high affinity for albumin, in mouse models. Under physiological conditions, albumin does not cross the endothelial barrier, and Evans Blue-bound albumin is restricted within blood vessels. In pathologic conditions with increased vascular permeability, the endothelium becomes permeable to small proteins such as albumin, and albumin-bound Evans Blue will appear in the organs with increased permeability. The extent of vascular permeability can be quantified by measuring the dye incorporated into the tissue. Evans blue dye (0.5%; Sigma-Aldrich, E2129) was prepared in PBS, and each mouse was injected with 200 μL of the solution (1.04 mM) via the tail vein. Thirty minutes post-injection, mice were euthanized, and heart tissue was harvested. Each sample was incubated in 500 μL of formamide at 55 °C for 24 hours to extract the dye. Vascular permeability was quantified by measuring the optical density of the extracted dye at 610 nm, as previously described [19].

2.9. Quantitative real-time polymerase chain reaction (qPCR)

Total RNA was extracted using the Quick-RNA MiniPrep Plus Kit (Zymo Research, CA, USA) and quantified with a NanoDrop 1000 spectrophotometer (Thermo Fisher, MA, USA). One microgram of RNA was reverse transcribed into cDNA using the Verso cDNA Synthesis Kit (Thermo Fisher, MA, USA), following the manufacturer's protocol. qPCR was then performed using the SsoAdvanced™ Universal SYBR® Green Supermix (Bio-Rad, USA) on a CFX96 Real-Time PCR Detection System (Bio-Rad, CA, USA). The primer sequence used were Cldn1 Forward (5'-TGA GTT GAA TAC CCC AGG CA-3') and Reverse (5'-GAC ATC CAC AGT CCC TCG TA-3'), GAPDH, forward (5'-TCC TGT TCG ACA GTC AGC CGC A-3') and reverse (5'-GCG CCC AAT ACG ACC AAA TCC GT-3'); CD163, forward (5'- TGC CTC TGC TGT CAC TAA CG -3') and reverse (5'- TTC ATT CAT GCT CCA GCC GT -3'); CD68, forward (5'- TTC TCC AGC TGT TCA CCT TGA CCT -3') and reverse (5'- GTT GCA AGA GAA ACA TGG CCC GAA -3'); F4/80 forward (5'- CCT GGA CGA ATC CTG TGA AG -3') and reverse (5'- GGT GGG ACC ACA GAG AGT TG -3'); eNOS, forward (5'- GTG ATG GCG AAG CGA GTG AAG G -3') and reverse (5'- ACC ACC AGC ACC AGC GTC TC -3'). The thermal cycling conditions consisted of an initial denaturation at 95 °C, followed by 39 amplification cycles, and melt-curve analysis from 65 °C to 95 °C to confirm amplification specificity. Threshold cycle (Ct) values were obtained for each gene, and mRNA expression was quantified using the Ct method, normalized to GAPDH as the endogenous control. Relative expression levels were calculated and expressed relative to control samples.

2.10. Western blot

HMVECs were washed with PBS, and heart tissue was finely ground prior to lysis in RIPA buffer (Thermo Fisher, 89900) supplemented with protease (Thermo Fisher, PI87786) and phosphatase inhibitors (Thermo Fisher, PI78420). Lysates were centrifuged at 1,000 g for 10 minutes at 4 °C, and supernatants were collected for protein quantification using a BCA Protein Assay Kit (Thermo Fisher, 23227). Equal amounts of protein were resolved on 4 – 20% gradient SDS PAGE gels (Bio Rad, 4561094) and transferred to PVDF membranes (Thermo Fisher, 88520). Membranes were blocked with 5% BSA (Fisher Scientific, BP1600 100) for 1 hour at room temperature and incubated overnight at 4 °C with primary antibodies against Cldn1 (EPR9306, Abcam, ab180158). After washing, the membranes were incubated with HRP-conjugated secondary antibodies for 1 hour at room temperature. After detection of Cldn1, membranes were reprobed with GAPDH as a loading control (mouse monoclonal anti-GAPDH antibody; clone 6C5; Santa Cruz Biotechnology, sc 32233; 1:5000 dilution). Protein bands were visualized using enhanced chemiluminescence (Thermo Scientific, 32106) on a ChemiDoc™ Imaging System (Bio Rad). Band intensities were quantified using ImageJ software. Cldn1 protein levels were normalized to the corresponding GAPDH loading control within the same lane, and data are presented as relative expression compared with control samples.

2.11. Tissue morphometry

For hematoxylin and eosin (H&E) staining, 4 m-thick sections from formalin-fixed, paraffin-embedded heart tissue were deparaffinized, rehydrated, stained with hematoxylin and eosin, dehydrated, and mounted. Images were acquired using a Leica Biosystem ScanScope® (Aperio Technologies, Vista, CA, USA) at 40x magnification and saved in TIFF format. Cardiomyocyte size and nuclear density were quantified using the ruler tool in ImageScope, specifically evaluating circular myocytes with centrally located nuclei. Masson's trichrome staining was performed using the Epredia™ Richard-Allan Scientific Masson Trichrome Kit (Epredia, 87109) according to the manufacturer's instructions. Slides were deparaffinized, rehydrated, and treated with Bouin's solution, and stained sequentially with Weigert's Iron Hematoxylin, Biebrich Scarlet-Acid Fuchsin, and Aniline Blue, then dehydrated and mounted. Collagen appeared blue, nuclei black, and myocardium red. Interstitial fibrosis was quantified using the Positive Pixel Count v9 algorithm in ImageScope, excluding perivascular regions using the negative pen tool. Trichrome staining was used to assess vascular and perivascular fibrosis in medium and small sized coronary vessels within the myocardium. Fibrosis quantification was performed using whole heart sections from each animal. Total vascular area and the area of positive fibrotic staining were measured using NIH ImageJ/Fiji software (National Institutes of Health, Bethesda, MD, USA). Coronary luminal size was determined using Fiji's measurement tools. Luminal area was initially measured in pixels² and converted to μm² using an adjusted conversion factor of 8.26 pixels²/μm². Because larger vessels exhibited proportionally greater fibrosis than smaller vessels, the fibrotic area was normalized to the corresponding luminal area.

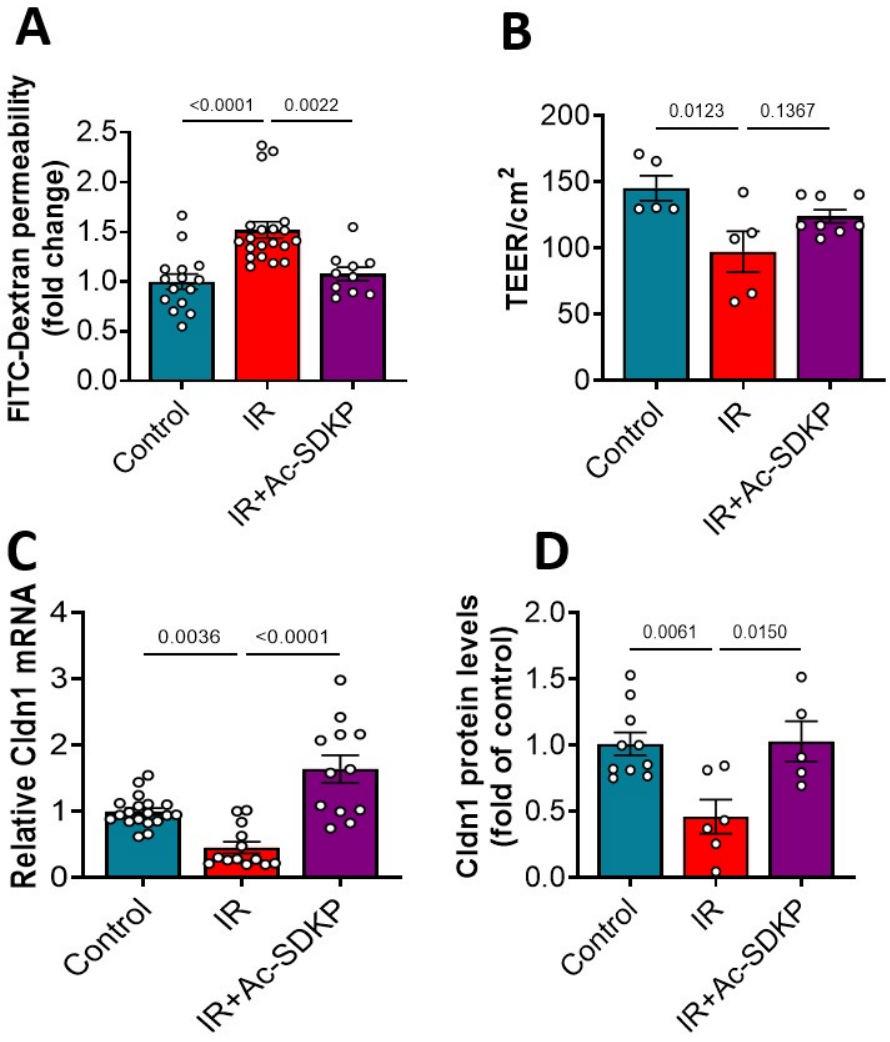

Figure 1: Effects of radiation and Ac-SDKP on coronary vascular endothelial cell (HMVEC) Cldn1 expression, vascular permeability, and endothelial barrier integrity. Radiation exposure (9 Gy) increased endothelial permeability, as measured by the FITC-dextran assay (A), and impaired endothelial barrier function, as indicated by a decrease in TEER (B). Similarly, radiation downregulated both mRNA (C) and protein levels (D) of Cldn1 in HMVECs. Ac-SDKP mitigated radiation-induced FITC-dextran permeability, but the effects on TEER were not statistically significant. All data are expressed as mean +/SEM, n=5-20.

2.12. Transmission Electron Microscopy (TEM)

Ultrastructural analysis was performed using a Hitachi HT7800 High-Resolution 120 kV Transmission Electron Microscope. Heart tissues were fixed overnight at room temperature in 2% formaldehyde and 2% EM-grade glutaraldehyde (Electron Microscopy Sciences, Hatfield, PA, USA) in 0.1 M cacodylate buffer (pH 7.2). After fixation, samples were washed in cacodylate buffer (without aldehydes) and post-fixed in 1% osmium tetroxide in 0.1 M cacodylate buffer for 1 hour. Tissues were then washed and dehydrated through a graded ethanol series (30%, 50%, 70%, and 95% for 10 minutes each), followed by two changes in 100% ethanol. Ultrathin sections were obtained, and images were acquired by an observer blinded to the experimental group from blood vessels of comparable size across conditions to allow comparison of ultrastructural features.

2.13. Statistical analysis

Results are expressed as means ± SEM, and analysis was done using GraphPad Prism software (version 9.0, GraphPad Software, San Diego, California, USA). The study was not powered to detect sex specific differences, and preliminary analyses did not reveal qualitative differences between sexes. Therefore, data were pooled across sex to focus on the primary experimental effects. For radial velocity analysis, peak systolic velocity, acceleration, and deceleration values from the six myocardial segments were averaged per animal to generate a single representative value prior to group-level statistical comparison. Quantitative endpoints were summarized by group using the mean and standard error of mean (SEM). When appropriate, endpoints were analyzed using an unpaired t-test or one-way ANOVA, with treatment group (control, radiation alone, and radiation + Ac-SDKP) as a factor. When significant effects were detected, pairwise between-group comparisons were conducted using Tukey's multiple comparisons test, based on a single pooled variance from the ANOVA model. P-values <0.05 were considered significant.

3. Results

3.1. Ac-SDKP inhibits radiation-induced vascular permeability in HMVECs

Radiation significantly increased endothelial permeability in HMVECs, as measured by FITC-dextran assay. Irradiated cells exhibited a 52%

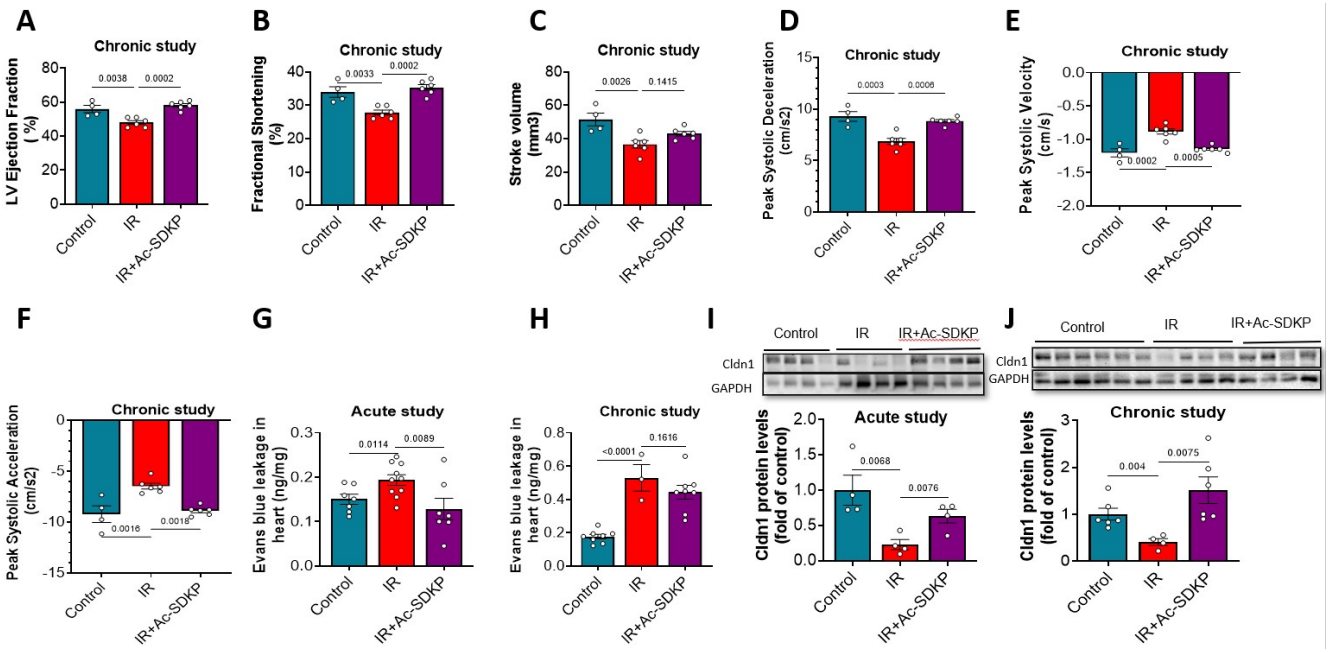

Figure 2: Effects of radiation and Ac-SDKP on cardiac function, cardiac vascular permeability, and Cldn1 levels. Radiation exposure (45 Gy, 15 fractions) impaired left ventricular ejection fraction (A), fractional shortening (B), stroke volume (C), peak systolic deceleration (D), peak systolic velocity (E), and peak systolic acceleration (F) in the chronic study model. Similarly, IR exposure increased Evans blue dye leakage (G, H) and decreased Cldn1 protein expression (I, J) in both acute and chronic models. These effects were mitigated by Ac-SDKP (3.2 mg/kg/day) in the acute setting, whereas the effect on cardiac vascular permeability was not statistically significant in the chronic setting. All data are expressed as mean +/SEM, n=3-9.

rise in permeability compared to controls (fluorescence intensity-relative expression: control, 1.00 ± 0.029; IR, 1.52±0.37; p<0.0001, n=15-20). Ac-SDKP treatment normalized permeability levels (0.71 ± 0.14; p = 0.0022 vs. IR, n = 9), indicating its role in preserving endothelial barrier function and membrane integrity **(Fig. 1A)**.

3.2. Effects on endothelial cell barrier integrity

Transendothelial electric resistance (TEER) measurements were performed, with 5 - 8 wells analyzed per condition across all experiments. Radiation significantly impaired endothelial barrier function, as evidenced by decreased TEER. Forty-eight hours after 9 Gy irradiation, TEER was reduced by approximately 33% in HMVECs (control: 145.3 ±21.12 vs. IR: 97.2 ±34.47; p = 0.0123, n=5). Pre-treatment with Ac SDKP was associated with a tendency to increase TEER in irradiated cells; however, this change did not reach statistical significance (IR + Ac SDKP: 123.86 ± 13.85 vs. IR: 97.2 ± 34.47; p = 0.1367, n = 5-8). Data are shown in **(Fig. 1B)**.

3.3. Ac-SDKP inhibits radiation-induced downregulation of Cldn-1 in HMVECs

Radiation exposure (9 Gy) significantly downregulated both mRNA and protein levels of Cldn1 in HMVECs. Compared to the control, irradiated cells showed a reduction of 55% in Cldn1 mRNA expression (relative expression: control, 1.00 ± 0.23; IR, 0.45 ± 0.31; p = 0.0036, n= 13-19) and a decrease of 54% in Cldn1 protein levels (relative expression: control, 1.00 ± 0.27; IR, 0.46 ± 0.31; p = 0.0061 n= 6-10) **(Figure 1)**. Treatment with Ac-SDKP restored Cldn1 expression (mRNA: 3.61± 0.68; p < 0.0001 vs. IR, n=12; protein: 2.24± 0.74; p = 0.015 vs. IR, n=5), suggesting a protective effect on the tight junction protein, which could contribute to membrane integrity following radiation **(Figs. 1C and 1D)**.

3.4. Effects of Ac-SDKP on radiation-induced cardiac damage

Cardiac MRI performed 19 weeks post-radiation revealed significant functional impairment in irradiated mice. Ejection fraction was reduced in irradiated mice but improved with Ac-SDKP therapy (control: 56.12±4.25%; IR: 48.05±2.67%; IR + Ac-SDKP: 58.23±2.63%; p = 0.0038, n= 4-6) **(Fig. 2A)**. Similarly, fractional shortening was reduced in irradiated mice but improved with Ac-SDKP therapy (control: 34.00±2.74%; IR: 27.83±1.67%; IR + Ac-SDKP: 35.33±1.97%; p = 0.0033 control vs IR and p= 0.0002 IR vs IR + Ac-SDKP, n=4-6) **(Fig. 2B)**. Stroke volume was reduced in the IR group compared to controls (control: 51.56±7.67 mm3; IR: 36.62±5.54 mm3; p = 0.0026, n= 4-6). Ac-SDKP treatment did not significantly improve stroke volume after IR (IR + Ac-SDKP: 43.04±3.36 mm3; p = 0.14, n=6) **(Fig. 2C)**. Radial velocity analysis demonstrated significant reductions in peak systolic velocity, peak systolic acceleration, and peak systolic deceleration following IR, all of which were improved by Ac-SDKP (deceleration: control: 9.30± 0.93 cm/s2; IR: 6.88 ± 0.73; IR + Ac-SDKP: 8.84± 0.37; p = 0.0003 control vs. IR, and 0.0006 IR vs. IR+ Ac-SDKP; velocity: control: -1.20 ± 0.12 cm/s; IR: -0.88 ± 0.10; IR + Ac-SDKP: -1.15± 0.05; p = 0.0002 control vs. IR, and 0.0005 IR vs. IR+ Ac-SDKP; acceleration: control: -9.20±1.63 cm/s2; IR: -6.45± 0.70; IR + Ac-SDKP: -8.87± 0.47; p = 0.0016 control vs. IR, and 0.0018 IR vs. IR+ Ac-SDKP, n=4-6) **(Fig. 2D-F)**.

3.5. Effects of Ac-SDKP on radiation-induced cardiac vascular leakage and Cldn1 levels

Radiation exposure (acute study) led to increased cardiac vascular permeability, demonstrated by a 29% increase in Evans blue dye extravasation compared to controls (ng/mg tissue: control: 0.15± 0.03; IR: 0.19 ± 0.04; p = 0.0114, n=7-10, indicating endothelial barrier disruption after 3 weeks. Treatment with Ac-SDKP significantly reduced cardiac vascular leakage in irradiated mice, restoring

permeability levels closer to baseline (IR + Ac-SDKP: 0.13±0.06; p =0.0089 vs IR, n=7) **(Fig. 2G)**. At 19 weeks, cardiac vascular permeability remained significantly elevated in irradiated animals compared to controls (ng/mg tissue: control: 0.18 ± 0.04; IR: 0.53 ± 0.14; p < 0.0001, n=3-8). Ac SDKP – treated irradiated mice showed a minor decrease in permeability compared to irradiated mice alone; however, this difference was not statistically significant (IR + Ac SDKP: 0.44 ± 0.12; IR vs. IR + Ac SDKP, p = 0.1616, n=8) **(Fig. 2H)**.

Radiation exposure significantly reduced cardiac Cldn1 expression in mice compared with non-irradiated controls at 3 weeks post-irradiation. Treatment with Ac-SDKP restored Cldn1 protein levels in irradiated animals (relative expression in densitometric units: control: 1.00 ± 0.42; IR: 0.23± 0.14; IR + Ac-SDKP: 0.63±0.19; p = 0.0068 control vs IR, p=0.0076 IR vs IR+ Ac-SDKP, n=4 each group) **(Fig. 2I)**. These effects of radiation and Ac-SDKP on Cldn1 protein levels persisted for 19 weeks after IR (relative expression in densitometric units: control: 1.00 ± 0.31; IR: 0.41± 0.14; IR + Ac-SDKP: 1.51±0.69; p = 0.004 control vs IR, p=0.0075 IR vs IR+ Ac-SDKP, n= 4-6) **(Fig. 2J)**.

3.6. Effects of IR and Ac-SDKP on fibroinflammatory response

To assess the impact of radiation and Ac-SDKP on macrophage-associated gene expression, we analyzed mRNA levels of CD68, F4/80, and CD163 in cardiac tissue at 3- and 19-weeks post-radiation.

At 3 weeks (acute phase), IR significantly increased CD163 expression compared to control (CD163: control, 1.00 ± 0.36; IR, 2.25 ± 1.27; p = 0.0035, n=4 per group), while CD68 (control, 1.00 ± 0.25; IR, 0.88 ± 0.07; p=NS, n=4 per group) and F4/80 (control, 1.00 ± 0.19; IR, 1.28 ± 0.37; p=NS, n=4 per group) levels remained unchanged. Treatment with Ac-SDKP significantly attenuated IR-induced CD163 expression (IR + Ac-SDKP, 0.26± 0.08; p = 0.0002 vs. IR, n=4 per group), with no significant effect on CD68 or F4/80 **(Fig. 3A)**. At 19 weeks (chronic phase), CD163 expression was significantly reduced in irradiated hearts compared to controls (CD163: control, 1.00 ± 0.19; IR, 0.07 ± 0.04; p = 0.0003, n=4-6), while F4/80 expression was increased (control, 1.00 ± 0.27; IR, 2.27 ± 0.82; p<0.0001, n=4-6). CD68 expression remained unchanged (control, 1.00 ± 0.21; IR, 1.22 ± 0.82; p = NS, n=4-6). Ac-SDKP did not alter CD163 levels (IR + Ac-SDKP, 1.31 ± 0.27; p = NS vs. IR, n=5) and CD68 mRNA levels (IR + Ac-SDKP, 0.97± 0.13; p = NS vs. IR, n=4), but significantly reduced F4/80 expression induced by radiation (IR + Ac-SDKP, 0.63 ± 0.20; p = 0.0016 vs. IR, n=5) **(Fig. 3B)**.

Additionally, after 3 weeks, IR decreased eNOS mRNA expression (control, 1.00 ± 0.23; IR, 0.74 ± 13; p = 0.0477), n=4 per group, while Ac-SDKP modestly increased eNOS levels, though not significantly (IR + Ac-SDKP, 1.29 ± 0.33; p = 0.08 vs. IR, n=4) **(Fig. 3C)**. As with the acute study, IR significantly suppressed eNOS expression (control, 1.00 ± 0.16; IR, 0.70 ± 0.08; p = 0.00380 n=4-6), and Ac-SDKP restored eNOS levels to near control values (IR + Ac-SDKP, 1.35 ± 0.28; p = 0.027, n=5) in chronic studies (19 weeks) **(Fig. 3D)**.

Radiation-induced fibrotic remodeling, however, was not evident either at 3 or 19 weeks as assessed by interstitial collagen deposition (interstitial collagen volume fraction at 3 weeks, fold of control: control: 1.00 ± 0.18; IR: 1.05± 0.07; IR + Ac-SDKP: 1.03± 0.31; p = NS, n=5-9; collagen volume fraction at 19-weeks post IR, fold of control: control: 1.00 ± 0.22; IR: 1.11± 0.20; IR + Ac-SDKP: 1.09± 0.27; p =NS, n=5-8) **(Fig. 3E-F)**, Similarly, Ac-SDKP treatment did not alter interstitial and perivascular fibrotic changes (relative % area stained at 19-weeks post IR: control: 1.00 ± 0.20; IR: 1.19±0.16; IR + Ac-SDKP: 1.35± 0.35; p =NS, n=5-9) **(Fig. 3G-H)**. Similarly, there was no significant difference in cardiomyocyte size or nuclear density across groups. Results are shown in **(Fig. 3I-K)**.

3.7. Electron microscopic findings

Electron microscopy revealed distinct ultrastructural changes in the coronary microvascular endothelium following radiation exposure and peptide treatment. In control hearts, endothelial cells displayed an intact and continuous basement membrane with well-apposed nuclei, indicating normal vascular ultrastructure. In contrast, hearts from irradiated mice showed marked endothelial damage, including nuclear dropout, and reduced basement membrane density, indicative of radiation-induced vascular injury. Notably, treatment with Ac-SDKP following irradiation preserved endothelial integrity. Endothelial nuclei remained visible, and the basement membrane exhibited increased density compared to irradiated hearts without treatment, suggesting a protective effect of the peptide against radiation-induced microvascular damage **(Figure 4)**. These observations, however, are descriptive in nature and reflect qualitative comparisons rather than quantitative morphometric assessment.

4. Discussion

Coronary vasculopathy is a well-known and serious complication of radiotherapy involving the thoracic region. While most prior research has examined post-radiation coronary artery atherosclerosis, the current study focuses on the coronary microvascular endothelial barrier dysfunction, with particular attention to the tight junction (TJ) protein Cldn1. This study identifies vascular barrier disruption as an early feature of radiation injury, and examines the association between Ac SDKP treatment, endothelial barrier-associated protein Cldn1, and functional outcomes. Using a combination of in vitro and in vivo experiments, we show that radiation exposure significantly disrupts endothelial tight junctions, impairs barrier function, and has partial, time-dependent downstream effects on cardiac function. Several of these radiation-associated changes were attenuated in the presence of Ac SDKP, although not uniformly across all endpoints.

Radiation-induced endothelial dysfunction is a well-recognized contributor to delayed cardiovascular complications after thoracic irradiation. Radiation injury leads to impaired endothelial functions such as reduced vasodilation, diminished capillary formation, and increased permeability [20, 21]. Previous studies have shown that ionizing radiation negatively affects endothelial cell integrity, which is expected given that endothelial cells are among the most radiosensitive cell types [22]. Endothelial cell paracellular permeability depends on tight junction (TJ) proteins, primarily the claudin and occludin families, as well as intracellular partners like JAM-2 and ZO-1, to maintain vessel wall integrity. Among these, Cldn1 plays a key role in maintaining the tight seal between endothelial cells, thereby preventing paracellular permeability [23]. Disruption or altered expression of Cldn1 in response to radiation can compromise endothelial barrier function and contribute to vascular dysfunction.

Our findings align with prior reports demonstrating that radiation disrupts epithelial cell tight junction proteins such as claudins, occludins, and ZO-1, leading to increased cell permeability and tissue injury[24]. We have previously noted that Cldn1 is expressed in coronary vascular endothelial cells and plays an important role in maintaining coronary vascular barrier integrity [8]. In the present study, Cldn1 expression was markedly reduced at both the mRNA and protein levels following radiation in human microvascular endothelial cells (HMVECs). Functionally, this was associated with increased paracellular permeability and reduced transendothelial electrical resistance (TEER), a marker of compromised endothelial

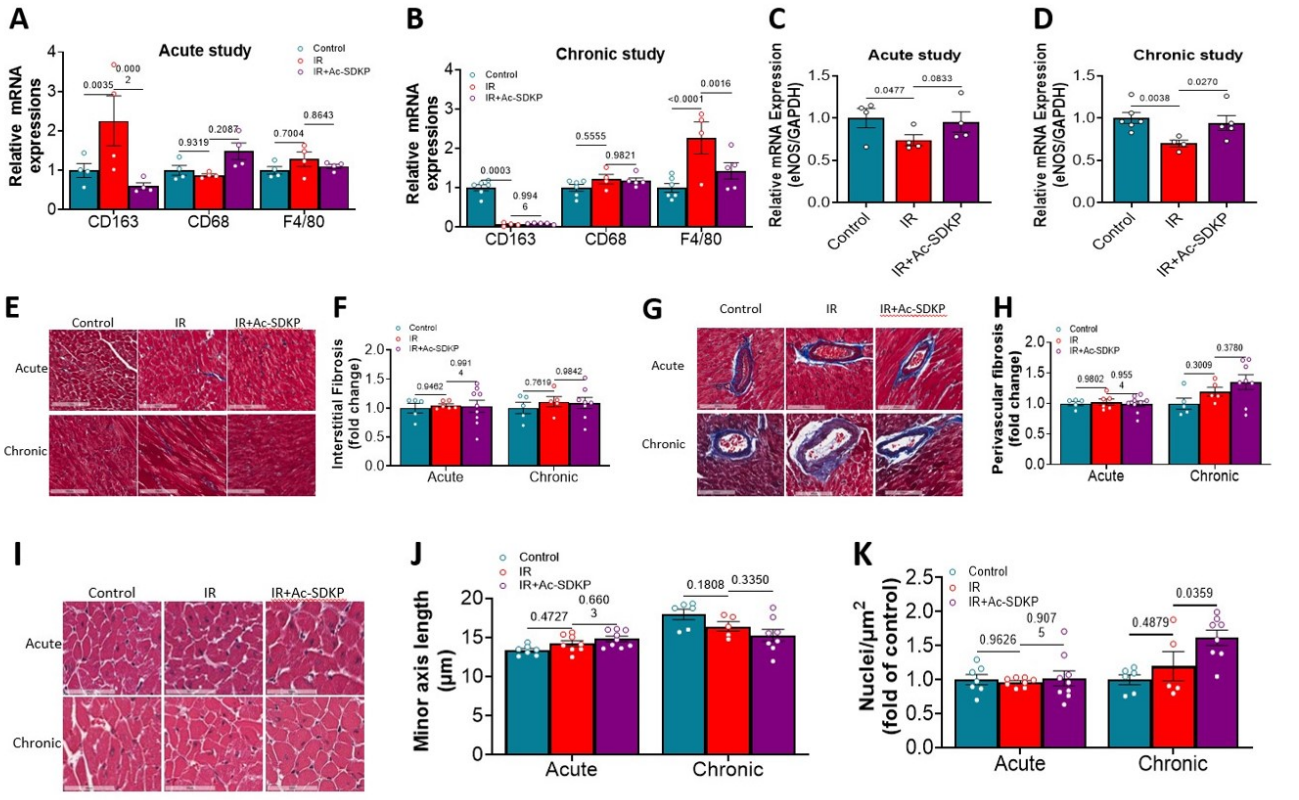

Figure 3: Effects of radiation and Ac-SDKP on fibroinflammatory response. Effects of radiation and Ac-SDKP on macrophage-associated inflammatory markers (CD163, CD68, and F4/80) in acute (A) and chronic (B) study models. mRNA expression of eNOS is shown for acute (C) and chronic (D) models. Representative trichrome-stained myocardial sections and quantification of interstitial (E–F) and perivascular (G–H) collagen are presented for both studies. Representative hematoxylin and eosin (H&E)–stained myocardial sections (I) illustrate cardiomyocyte morphology, with no significant differences observed in cardiomyocyte size (J) or nuclear density (K) among groups. All data are expressed as mean +/SEM, n=4-9.

barrier integrity. Notably, treatment with Ac-SDKP restored Cldn1 levels and normalized endothelial permeability, suggesting that Ac-SDKP may protect tight junctions and membrane integrity after radiation injury. It should, however, be emphasized that Ac SDKP treatment was associated with higher Cldn1 expression and decreased endothelial cell permeability (in HMVECs); the recovery of TEER did not reach statistical significance, underscoring the partial nature of this effect. Since we did not use a genetic loss-of-function or gain-of-function model, Cldn1 preservation in this context should be interpreted as a parallel observation that reflects barrier status, rather than as direct evidence of a mechanistic pathway.

In vivo, irradiated mice exhibited increased coronary vascular permeability, sustained reductions in Cldn1 protein levels, and impaired cardiac function, as measured by ejection fraction, fractional shortening, and radial strain. Ac SDKP treatment was associated with improved early permeability measures and selected MRI parameters; however, chronic permeability reduction did not reach statistical significance. These findings are consistent with our prior studies implicating endothelial damage and microvascular rarefaction in the pathogenesis of radiation-induced cardiomyopathy [16] while also highlighting that the degree of protection observed here is incomplete and time-dependent.

Previous studies using electron microscopy have demonstrated that radiation induces profound ultrastructural changes in cardiac microvascular endothelium. In rabbit models exposed to 10 – 13 Gy, investigators reported increased pinocytic vesicle transport across endothelial cells along intercellular junctional gaps and disruption of endothelial sheets, as evidenced by leakage of carbon particles [25, 26]. Additionally, elevated endothelial phagocytic activity, including erythrophagocytosis, was observed in a dose-dependent manner [27]. These findings provided early evidence that radiation impairs both intracellular trafficking and intercellular connectivity, contributing to increased vascular permeability. Consistent with these reports, our electron microscopy analysis revealed hallmark features of radiation-induced endothelial injury in the heart, including nuclear dropout, thinning and rarefaction of basement membranes, and focal loss of basement membrane continuity. In AcSDKP – treated irradiated hearts, ultrastructural features appeared qualitatively less severe, with preserved endothelial nuclei and a continuous basement membrane. However, these observations are descriptive in nature, based on blinded image acquisition from vessels of comparable size, and were not supported by morphometric quantification. Therefore, TEM findings are presented as supportive evidence rather than definitive mechanistic proof.

The protective role of Ac-SDKP in radiation-induced cardiovascular injury is supported by prior studies demonstrating its antifibrotic, anti-inflammatory, and endothelial-protective properties in various models of cardiac injury [14, 15, 28, 29]. Mechanistically, Ac-SDKP is known to enhance endothelial nitric oxide synthase (eNOS) activity, inhibit TGF- signaling, and reduce reactive oxygen species, all of which may contribute to its effects observed here [13, 17, 30].

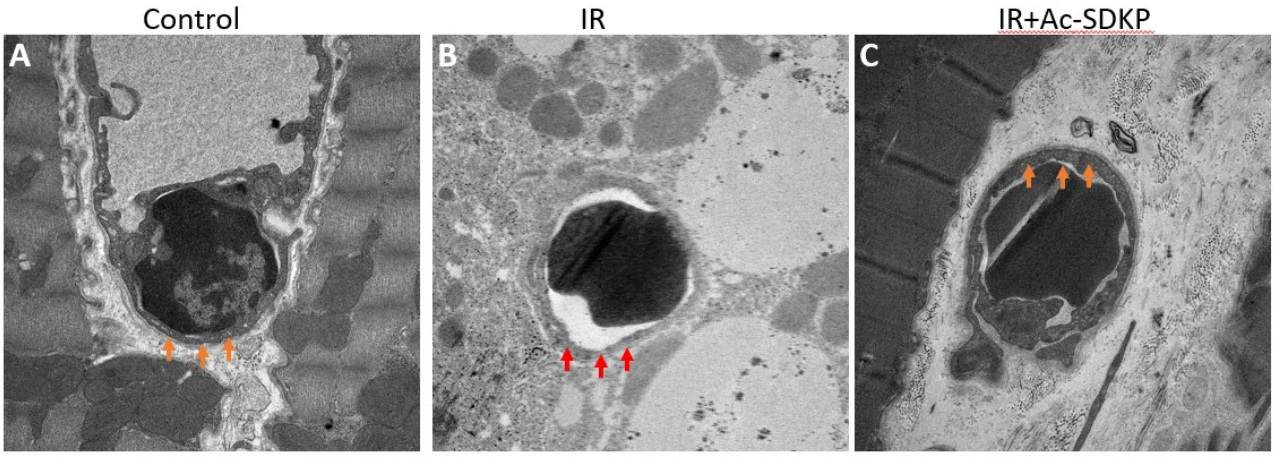

Figure 4: Effects of radiation and Ac-SDKP on the myocardial coronary vasculature examined by transmission electron microscopy (acute study). Representative images from control, IR, and IR + Ac-SDKP–treated mouse hearts show coronary vasculature with radiation-induced endothelial injury characterized by nuclear dropout and reduced basement membrane density. Treatment with Ac-SDKP mitigated these changes. Denser basement membranes are indicated by orange arrows, and paler basement membranes by red arrows.

In the present study, molecular markers such as eNOS and selected inflammatory transcripts, including CD163 and F4/80, increased with radiation exposure and decreased with AcSDKP treatment, suggesting an anti-inflammatory response; however, these data do not establish immune cell infiltration or phenotype at the tissue level.

Interestingly, despite the evidence of vascular injury, we did not observe significant interstitial or perivascular fibrosis at either 3 or 19 weeks, nor changes in cardiomyocyte size or nuclear density. This suggests that the injury phenotype captured here represents a vascular dominant and pre fibrotic stage of radiation-induced cardiac injury. Unlike the rat model, in which interstitial fibrosis is prominent at 18 weeks after IR [17], the mouse model appears more resistant to fibrosis. This temporal pattern is consistent with prior reports indicating that overt radiation-induced fibrosis in mice typically emerges at later time points, often beyond 24 weeks post-irradiation [31]. The absence of fibrosis in this study, therefore, likely reflects the examined time frame rather than inconsistency with established models. Furthermore, cardiomyocyte hypertrophy and nuclear density were unchanged across groups, suggesting that early cardiac dysfunction in this context is driven primarily by vascular mechanisms rather than myocyte remodeling. These findings align with earlier reports indicating minimal effects on cardiomyocyte size or BNP expression after radiation injury in some animal models [32].

Several limitations should be acknowledged. This study was preventive in design and did not evaluate Ac SDKP as a therapeutic intervention after established injury, nor did it include a dose-response analysis or an Ac SDKP-only control arm. Although associations between Cldn1 expression, vascular permeability, and functional outcomes were observed, no targeted mechanistic interventions were performed to establish causality. Because radiation was delivered unilaterally while outcomes were assessed at the whole heart level, regional effects may be diluted in global analyses. Accordingly, the findings reflect integrated whole heart consequences of localized radiation exposure rather than spatially resolved regional pathology. Whole-heart lysates and permeability assays were used to limit endothelial specificity, and permeability was assessed using Evans blue uptake as a surrogate for coronary leakage. LV volumes and ejection fraction were derived from a single mid-ventricular short-axis cine acquisition rather than a contiguous short-axis stack with disk summation. This approach is appropriate given the absence of regional wall-motion abnormalities in this model, but it is a limitation; future studies should incorporate whole-LV volumetry. Ultrastructural analyses were qualitative, and inflammatory assessments relied on bulk gene expression rather than cell level validation. Collectively, these constraints limit mechanistic inference and translational extrapolation.

5. Conclusions

In summary, this study identifies disruption of the cardiac vascular barrier as an early feature of radiation-associated cardiac injury and demonstrates that preventive Ac-SDKP administration reduces cardiac vascular leakage and partially preserves cardiac function in experimental models. Changes in Cldn1 expression closely paralleled alterations in vascular permeability, supporting its utility as a marker of endothelial barrier status. However, because direct genetic or pharmacologic manipulation of Cldn1 was not performed, these observations should be interpreted as correlative rather than causal. Accordingly, Cldn1 is best considered a candidate pathway associated with barrier regulation in this context. Future studies incorporating targeted mechanistic interventions and endothelial specific analyses will be required to define causal relationships and assess translational relevance.

Conflicts of Interest

The authors declare no competing interests that could have influenced the objectivity or outcome of this research.

Funding Source

Roswell Park and the National Cancer Institute supported this research under award number P30CA016056. S.P. is supported by a grant from NIH/NHLBI (Grant No. R01HL150266). U.C.S is supported by a grant from NIH/NHLBI (Grant R01HL152090).

Acknowledgments

None.

Institutional Review Board (IRB)

All animal experiments were approved by the Institutional Animal Care and Use Committee (IACUC) of Roswell Park Comprehensive Cancer Center and conducted in accordance with institutional guidelines.

Large Language Model

During the preparation of this work, the author(s) used ChatGPT to edit the language. After using this tool/service, the author(s) reviewed and edited the content as needed and take full responsibility for the content of the publication.

Author Contributions

SN contributed to methodology, validation, formal analyses, investigation, and writing the original draft, SDS participated in methodology and investigation, BK contributed to analyses of imaging data, JS provided image acquisition and resources, SDM was responsible for in vitro experimental resources, review, and editing, UCS contributed to conceptualization, review, and editing, SP led conceptualization, funding acquisition, supervision, and review and editing.

Data Availability

Raw data generated and included in this article are available upon reasonable request.

References

1. Miller KD, Siegel RL, Lin CC, Mariotto AB, Kramer JL, Rowland JH, et al. Cancer treatment and survivorship statistics, 2016. CA Cancer J Clin. 2016;66(4):271-89. [PMID: 27253694, https://doi.org/10.3322/caac.21349].
2. Aronow H, Kim M, Rubenfire M. Silent ischemic cardiomyopathy and left coronary ostial stenosis secondary to radiation therapy. Clin Cardiol. 1996;19(3):260-2. [PMID: 8674269, https://doi.org/10.1002/clc.4960190325].
3. Abe JI, Allen BG, Beyer AM, Lewandowski D, Mapuskar KA, Subramanian V, et al. Radiation-Induced Macrovessel/Microvessel Disease. Arterioscler Thromb Vasc Biol. 2024;44(12):2407-15. [PMID: 39445428, PMCID: PMC11842029, https://doi.org/10.1161/ATVBAHA.124.319866].
4. Komarova YA, Kruse K, Mehta D, Malik AB. Protein Interactions at Endothelial Junctions and Signaling Mechanisms Regulating Endothelial Permeability. Circ Res. 2017;120(1):179-206. [PMID: 28057793, PMCID: PMC5225667, https://doi.org/10.1161/CIRCRESAHA.116.306534].
5. Lee WL, Slutsky AS. Sepsis and endothelial permeability. N Engl J Med. 2010;363(7):689-91. [PMID: 20818861, https://doi.org/10.1056/NEJMcibr1007320].
6. Furuse M, Hata M, Furuse K, Yoshida Y, Haratake A, Sugitani Y, et al. Claudin-based tight junctions are crucial for the mammalian epidermal barrier: a lesson from claudin-1-deficient mice. J Cell Biol. 2002;156(6):1099-111. [PMID: 11889141, PMCID: PMC2173463, https://doi.org/10.1083/jcb.200110122].
7. Xia Y, Cao H, Zheng J, Chen L. Claudin-1 Mediated Tight Junction Dysfunction as a Contributor to Atopic March. Front Immunol. 2022;13:927465. [PMID: 35844593, PMCID: PMC9277052, https://doi.org/10.3389/fimmu.2022.927465].
8. Nepali S, Chen M, Karthikeyan B, Sonkawade SD, Mahajan SD, Spernyak J, et al. Claudin 1 dysregulation disrupts coronary microvascular integrity and impairs cardiac function. Atherosclerosis. 2025;403:119149. [PMID: 40068507, PMCID: PMC12070307, https://doi.org/10.1016/j.atherosclerosis.2025.119149].
9. Vasques-Novoa F, Angelico-Goncalves A, Alvarenga JMG, Nobrega J, Cerqueira RJ, Mancio J, et al. Myocardial oedema: pathophysiological basis and implications for the failing heart. ESC Heart Fail. 2022;9(2):958-76. [PMID: 35150087, PMCID: PMC8934951, https://doi.org/10.1002/ehf2.13775].
10. Cavasin MA, Rhaleb NE, Yang XP, Carretero OA. Prolyl oligopeptidase is involved in release of the antifibrotic peptide Ac-SDKP. Hypertension. 2004;43(5):1140-5. [PMID: 15037553, PMCID: PMC4677773, https://doi.org/10.1161/01.HYP.0000126172.01673.84].
11. Azizi M, Ezan E, Nicolet L, Grognet JM, Menard J. High plasma level of N-acetyl-seryl-aspartyl-lysyl-proline: a new marker of chronic angiotensin-converting enzyme inhibition. Hypertension. 1997;30(5):1015-9. [PMID: 9369248, https://doi.org/10.1161/01.hyp.30.5.1015].
12. Lenfant M, Wdzieczak-Bakala J, Guittet E, Prome JC, Sotty D, Frindel E. Inhibitor of hematopoietic pluripotent stem cell proliferation: purification and determination of its structure. Proc Natl Acad Sci U S A. 1989;86(3):779-82. [PMID: 2915977, PMCID: PMC286560, https://doi.org/10.1073/pnas.86.3.779].
13. Sonkawade SD, Xu S, Kim M, Nepali S, Karambizi VG, Sexton S, et al. Phospholipid Encapsulation of an Anti-Fibrotic Endopeptide to Enhance Cellular Uptake and Myocardial Retention. Cells. 2023;12(12). [PMID: 37371059, PMCID: PMC10296995, https://doi.org/10.3390/cells12121589].
14. Peng H, Carretero OA, Vuljaj N, Liao TD, Motivala A, Peterson EL, et al. Angiotensin-converting enzyme inhibitors: a new mechanism of action. Circulation. 2005;112(16):2436-45. [PMID: 16216963, PMCID: PMC6824430, https://doi.org/10.1161/CIRCULATIONAHA.104.528695].
15. Pokharel S, van Geel PP, Sharma UC, Cleutjens JP, Bohnemeier H, Tian XL, et al. Increased myocardial collagen content in transgenic rats overexpressing cardiac angiotensin-converting enzyme is related to enhanced breakdown of N-acetyl-Ser-Asp-Lys-Pro and increased phosphorylation of Smad2/3. Circulation. 2004;110(19):3129-35. [PMID: 15520311, https://doi.org/10.1161/01.CIR.0000147180.87553.79].
16. Sharma UC, Sonkawade SD, Baird A, Chen M, Xu S, Sexton S, et al. Effects of a novel peptide Ac-SDKP in radiation-induced coronary endothelial damage and resting myocardial blood flow. Cardiooncology. 2018;4. [PMID: 31057947, PMCID: PMC6497419, https://doi.org/10.1186/s40959-018-0034-1].
17. Sharma UC, Sonkawade SD, Spernyak JA, Sexton S, Nguyen J, Dahal S, et al. A Small Peptide Ac-SDKP Inhibits Radiation-Induced Cardiomyopathy. Circ Heart Fail. 2018;11(8):e004867. [PMID: 30354563, PMCID: PMC6205206, https://doi.org/10.1161/CIRCHEARTFAILURE.117.004867].
18. Karthikeyan B, Sonkawade SD, Pokharel S, Preda M, Schweser F, Zivadinov R, et al. Tagged cine magnetic resonance imaging to quantify regional mechanical changes after acute myocardial infarction. Magn Reson Imaging. 2020;66:208-18. [PMID: 31668928, PMCID: PMC7031039, https://doi.org/10.1016/j.mri.2019.09.010].
19. Radu M, Chernoff J. An in vivo assay to test blood vessel permeability. J Vis Exp. 2013;(73):e50062. [PMID: 23524912, PMCID: PMC3639515, https://doi.org/10.3791/50062].
20. Beckman JA, Thakore A, Kalinowski BH, Harris JR, Creager MA. Radiation therapy impairs endothelium-dependent vasodilation in humans. J Am Coll Cardiol. 2001;37(3):761-5. [PMID: 11693749, https://doi.org/10.1016/s0735-1097(00)01190-6].
21. Suvorava T, Luksha LS, Lobanok LM. The effects of acute and chronic radiation on endothelium- and no-dependent vascular reactivity. Cell Mol Biol (Noisy-le-grand). 2005;51(3):321-7. [PMID: 16191400].
22. Reinhold HS, Buisman GH. Radiosensitivity of capillary endothelium. Br J Radiol. 1973;46(541):54-7. [PMID: 4683331, https://doi.org/10.1259/0007-1285-46-541-54].
23. Gunzel D, Fromm M. Claudins and other tight junction proteins. Compr Physiol. 2012;2(3):1819-52. [PMID: 23723025,

https://doi.org/10.1002/cphy.c110045].

24. Shukla PK, Gangwar R, Manda B, Meena AS, Yadav N, Szabo E, et al. Rapid disruption of intestinal epithelial tight junction and barrier dysfunction by ionizing radiation in mouse colon in vivo: protection by N-acetyl-l-cysteine. Am J Physiol Gastrointest Liver Physiol. 2016;310(9):G705-15. [PMID: 26822914, PMCID: PMC4867328, https://doi.org/10.1152/ajpgi.00314.2015].
25. Khan MY, Ohanian M. Radiation-Induced Cardiomyopathy: II. An Electron Microscopic Study of Myocardial Microvasculature. Am J Pathol. 1974;74(1):125-36. [PMID: 19971051, PMCID: PMC1910718].
26. RM B, , EF Y, , R S, , et al. Effects of radiation on endothelial barrier and vascular integrity. Tissue Barriers in Disease, Injury and Regeneration. 2021:43–94.
27. Bari WA, Sorenson GD. Ultrastructural Alterations in X-Irradiated Spleen. Pathol Microbiol (Basel). 1964;27:257-75. [PMID: 14132879, https://doi.org/10.1159/000161473].
28. Peng H, Xu J, Yang XP, Kassem KM, Rhaleb IA, Peterson E, et al. N-acetyl-seryl-aspartyl-lysyl-proline treatment protects heart against excessive myocardial injury and heart failure in mice. Can J Physiol Pharmacol. 2019;97(8):753-65. [PMID: 30998852, PMCID: PMC6824427, https://doi.org/10.1139/cjpp-2019-0047].
29. Sharma U, Rhaleb NE, Pokharel S, Harding P, Rasoul S, Peng H, et al. Novel anti-inflammatory mechanisms of N-Acetyl-Ser-Asp-Lys-Pro in hypertension-induced target organ damage. Am J Physiol Heart Circ Physiol. 2008;294(3):H1226-32. [PMID: 18178715, PMCID: PMC6824420, https://doi.org/10.1152/ajpheart.00305.2007].
30. Pokharel S, Rasoul S, Roks AJ, van Leeuwen RE, van Luyn MJ, Deelman LE, et al. N-acetyl-Ser-Asp-Lys-Pro inhibits phosphorylation of Smad2 in cardiac fibroblasts. Hypertension. 2002;40(2):155-61. [PMID: 12154106, https://doi.org/10.1161/01.hyp.0000025880.56816.fa].
31. Dreyfuss AD, Goia D, Shoniyozov K, Shewale SV, Velalopoulou A, Mazzoni S, et al. A Novel Mouse Model of Radiation-Induced Cardiac Injury Reveals Biological and Radiological Biomarkers of Cardiac Dysfunction with Potential Clinical Relevance. Clin Cancer Res. 2021;27(8):2266-76. [PMID: 33542079, PMCID: PMC9215266, https://doi.org/10.1158/1078-0432.CCR-20-3882].
32. Tokatli F, Uzal C, Doganay L, Kocak Z, Kaya M, Ture M, et al. The potential cardioprotective effects of amifostine in irradiated rats. Int J Radiat Oncol Biol Phys. 2004;58(4):1228-34. [PMID: 15001267, https://doi.org/10.1016/j.ijrobp.2003.09.071].